Shi, B.; Bartels, A.; Mosler, J.:

On the thermodynamically consistent modeling of distortional hardening: A novel generalized framework

In: International Journal of Plasticity (2014) Elsevier

DOI: 10.1016/j.ijplas.2014.05.008

On the thermodynamically consistent modeling of distortional hardening: A novel generalized framework

Baodong Shi[a], Alexander Bartels[a], Jörn Mosler[a,b,*]

[a] *TU Dortmund, Institute of Mechanics, Leonhard-Euler-Straße 5, D-44227 Dortmund, Germany*
[b] *Helmholtz-Zentrum Geesthacht, Institute of Materials Research, Materials Mechanics, D-21502 Geesthacht, Germany*

Abstract

Many important physical effects of materials undergoing plasticity at the macroscale cannot be captured realistically by isotropic and kinematic hardening only. For instance, the evolution of the texture in polycrystals results macroscopically in a distorted yield surface. This paper deals with adequate hardening models for such a distortion. To be more precise, a novel general frame for finite strain plasticity models is elaborated. To the best knowledge of the authors, it is the first one combining the following features: (1) proof of thermodynamical consistency; (2) decomposition of distortional hardening into dynamic hardening (due to currently active dislocations) and latent hardening (due to currently inactive dislocations); (3) difference of the yield surface's curvature in loading direction and in the opposite direction. The cornerstone of this model is a new plastic potential for the evolution equations governing distortional hardening. Although this type of hardening is characterized through a fourth-order tensor as internal variable, the structure of the aforementioned potential is surprisingly simple. Even though the final model is rather complex, it requires only few model parameters. For these parameters, in turn, physically sound bounds based on the convexity condition of the yield surface can be derived. Three different examples demonstrate the predictive capabilities of the novel framework.

Keywords: Distortional hardening; dynamic hardening; latent hardening; generalized standard materials; finite strain plasticity theory

*Corresponding author. Tel.: +49 231 755 5744
URL: joern.mosler@udo.edu (Jörn Mosler)

1. Introduction

Although a certain trend towards a micromechanical description of polycrystals can indeed be observed in the literature, cf. e.g. Homayonifar and Mosler (2012); Miehe et al. (2002), macroscopic models are still most frequently applied, if problems at the technologically most relevant scale are to be analyzed, see Nebebe et al. (2009); Mekonen et al. (2012) and references cited therein. The reason for this is their numerical efficiency. However, this positive feature is accompanied with a high complexity of the underlying constitutive model. To be more precise and focusing on polycrystals, the macroscopic model has to capture effects (in the sense of homogenization theory) due to the rotation of the atomic lattice within the individual grains as well as the distortion (e.g., elongation) of the grains. In many cases that cannot be realized by isotropic and kinematic hardening models only, since the aforementioned effects often lead to a distortion of the macroscopic yield surface. Models accounting for this transformation are referred to as *distortional hardening models*. A broad variety of these approaches can be found, e.g., in Baltov and Sawczuk (1965); Ortiz and Popov (1983); Haddadi et al. (2006); Feigenbaum and Dafalias (2007, 2008); Barthel et al. (2008); Noman et al. (2010); Shi and Mosler (2013). Most of these approaches are based on evolution equations for a fourth-order tensor describing the plastic material symmetry of the material, cf. Baltov and Sawczuk (1965); Dafalias (1979); Ortiz and Popov (1983); Feigenbaum and Dafalias (2007); Barthel et al. (2008); Noman et al. (2010).

A comprehensive overview and comparison of some distortional hardening models are presented in Shi and Mosler (2013). According to this paper, most models share one similarity: distortional hardening is governed by an Armstrong-Frederick-type evolution equation. Despite this fundamental similarity, the models are significantly different, and therefore their range of applications also differs. In order to explain these differences, the most important physical effects and their influence on the macroscopic yield surface are summarized in Fig. 1. In all figures, a uniaxial tension test is considered. Fig. 1a) shows the typical dynamic hardening effect. At the microscale, currently active dislocations lead to this phenomenon at the macroscale. Depending on the material, the opposite effect, i.e., dynamic softening, can also arise. In addition to an elongation/shrinkage of the yield surface in loading direction, the orthogonal direction can also undergo (cross) hardening/softening. This is depicted in Fig. 1b). Particularly for materials showing a pronounced variation of the Lankford coefficient (r-value), an uncoupling of dynamic and latent hardening is important. Physically speaking, latent hardening is due to currently inactive dislocations which have to be crossed by the active ones and thereby yield additional hardening. Finally, for some materials such as high-strength aluminum alloys, a

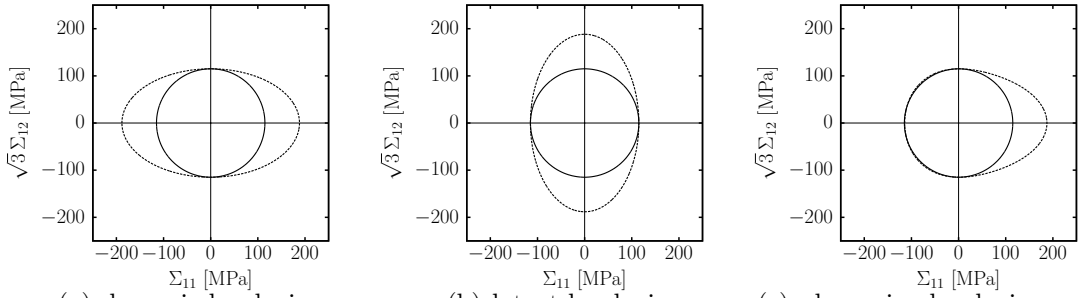

(a) dynamic hardening (b) latent hardening (c) dynamic hardening with high curvature along loading direction

Figure 1: Sketch of yield surface evolution with distortional hardening

higher curvature of the yield function is observed in loading direction in contrast to the reverse direction. This special type of dynamic hardening is outlined in Fig. 1c). To the best knowledge of the authors, only one of the existing constitutive models in the literature covers all of the aforementioned phenomena, cf. Pietryga et al. (2012). However, thermodynamical consistency of this models is not proven.

Within the models advocated in Baltov and Sawczuk (1965); Dafalias (1979); Ortiz and Popov (1983); Feigenbaum and Dafalias (2007, 2008); Shi and Mosler (2013), dynamic and latent hardening are captured by means of only one evolution equation. Although this simplicity is indeed appealing, such an approach is usually too restrictive for real materials. To be more precise, the implied coupling between latent and dynamic hardening does not agree with the results observed in many experiments.

Models accounting for a different response of dynamic and latent hardening are discussed in Peeters et al. (2002); Haddadi et al. (2006); Barthel et al. (2008); Noman et al. (2010). Conceptually, two independent evolution equations governing dynamic and latent hardening are introduced for that purpose. By doing so, the so-called *cross hardening effect* can be captured more realistically. Although the cited models do improve the predictive capabilities of the cross hardening effect, thermodynamically consistency has not been proven yet. Furthermore, the stress space implied by the evolution equations in Barthel et al. (2008); Noman et al. (2010) can be unbounded, resulting in stresses of infinite magnitude. These effects will be analyzed in detail in the present paper.

Within the third class of distortional hardening models, a higher curvature of the yield function in loading direction compared to the reverse direction is incorporated, cf. Ortiz and Popov (1983); Feigenbaum and Dafalias (2007, 2008). This is realized

by coupling distortional and kinematic hardening. Such a coupling is important for the modeling of high-strength aluminum alloys for instance.

The concise review of existing distortional hardening models shows that a model capturing the distortion of the yield surface due to latent and dynamic hardening for which thermodynamical consistency is explicitly shown, is still missing. Such a missing unified framework is elaborated in the present paper. This framework falls into the range of so-called *generalized standard materials* in the sense of Mandel (1971); Lemaitre (1985) and thus, the second law of thermodynamics is automatically fulfilled. Furthermore, the effect of a higher curvature of the yield surface in loading direction can be incorporated directly into this framework. In this respect, the novel model unifies the approach proposed in Feigenbaum and Dafalias (2007, 2008) and that suggested in Barthel et al. (2008); Noman et al. (2010). Physical bounds of the model parameters related to distortional hardening are derived by analyzing convexity of the saturated yield surface.

The paper is organized as follows: Section 2 gives a concise summary of finite strain plasticity theory and presents a prototype model which accounts for isotropic and kinematic hardening. Distortional hardening models are the focus of Section 3. Existing models are reviewed first. Subsequently, a novel constitutive model showing the aforementioned properties is elaborated (decomposition of distortional hardening into dynamic and latent parts; thermodynamical consistency). The applicability of the final model is demonstrated in Section 4 by means of numerical examples.

2. Plasticity theory in a nutshell

2.1. Fundamentals

In line with the most frequently applied plasticity frameworks such as those proposed and discussed in Lee (1969); Coleman and Gurtin (1967); Simo and Hughes (1998); Simo (1998); Xiao et al. (2000); Bruhns et al. (1999); Mandel (1971); Lemaitre (1985), the deformation gradient $\boldsymbol{F} := \mathrm{GRAD}\boldsymbol{\varphi}$ is multiplicatively decomposed into an elastic part $\boldsymbol{F}^{\mathrm{e}}$ and into a plastic part $\boldsymbol{F}^{\mathrm{p}}$, i.e.,

$$\boldsymbol{F} = \boldsymbol{F}^{\mathrm{e}} \cdot \boldsymbol{F}^{\mathrm{p}}, \qquad \text{with} \qquad \det \boldsymbol{F}^{\mathrm{e}} > 0, \ \det \boldsymbol{F}^{\mathrm{p}} > 0. \tag{1}$$

Since constitutive models suitable for analyzing plastic deformation are usually based on evolution equations for the inelastic strains $\boldsymbol{F}^{\mathrm{p}}$, deformation rates are also required. Analogously to the standard spatial velocity gradient

$$\boldsymbol{l} := \dot{\boldsymbol{F}} \cdot \boldsymbol{F}^{-1} \tag{2}$$

the two additional velocity gradients

$$\boldsymbol{L}^{\mathrm{p}} := \dot{\boldsymbol{F}}^{\mathrm{p}} \cdot [\boldsymbol{F}^{\mathrm{p}}]^{-1}, \qquad \boldsymbol{l}^{\mathrm{e}} := \dot{\boldsymbol{F}}^{\mathrm{e}} \cdot [\boldsymbol{F}^{\mathrm{e}}]^{-1} \tag{3}$$

are therefore defined. In Eqs. (2) and (3), the superposed dot represents the material time derivative.

The constitutive response is then defined. Within a thermodynamical framework, such a response can be conveniently described by means of a Helmholtz energy Ψ. Following the underlying assumptions of the kinematics (1), the Helmholtz energy Ψ is also decomposed into an elastic part Ψ^{e} (due to elastic distortion of the atomic lattice) and a plastic part Ψ^{p} (due to plastic work and hardening). To be more precise,

$$\Psi = \Psi^{\mathrm{e}}(\boldsymbol{F}^{\mathrm{e}}) + \Psi^{\mathrm{p}}(\boldsymbol{\alpha}). \tag{4}$$

In this paper, Ψ^{p} will cover isotropic, kinematic hardening as well as distortional hardening (distortion of the yield function). Application of the meanwhile standard Coleman & Noll procedure (see Coleman and Gurtin (1967)) yields the stress response

$$\boldsymbol{P} = \partial_{\boldsymbol{F}} \Psi \tag{5}$$

and the reduced dissipation inequality

$$\mathcal{D} = \boldsymbol{\Sigma} : \boldsymbol{L}^{\mathrm{p}} + \boldsymbol{Q} \cdot \dot{\boldsymbol{\alpha}} \geq 0, \qquad \boldsymbol{Q} := -\partial_{\boldsymbol{\alpha}} \Psi \tag{6}$$

where $\boldsymbol{P}$ is the first Piola-Kirchhoff stress tensor, $\boldsymbol{\Sigma} = 2\,\boldsymbol{C}^{\mathrm{e}} \cdot \partial_{\boldsymbol{C}^{\mathrm{e}}} \Psi$ is the Mandel stress tensor and $\boldsymbol{Q}$ is the stress-like internal variable energetically conjugate to $\boldsymbol{\alpha}$.

The dissipation inequality (6) is trivially fulfilled for elastic unloading ($\boldsymbol{L}^{\mathrm{p}} = \boldsymbol{0}$ and $\dot{\boldsymbol{\alpha}} = \boldsymbol{0}$). In order to derive evolution equations which also fulfill the dissipation inequality (6) in the case of plastic loading, the framework of *generalized standard materials* is adopted here, cf. Mandel (1971); Lemaitre (1985). Within this framework, the evolution equations are the generalized gradients of a suitable convex and non-negative plastic potential g, i.e., the flow rule and the hardening rules are chosen to be

$$\boldsymbol{L}^{\mathrm{p}} = \lambda\, \partial_{\boldsymbol{\Sigma}} g \qquad \dot{\boldsymbol{\alpha}} = \lambda\, \partial_{\boldsymbol{Q}} g. \tag{7}$$

In Eq. (7), $\lambda \geq 0$ is the non-negative plastic multiplier. The convexity of g, together with $g \geq 0$ and $g(\boldsymbol{0}) = 0$, clearly implies that $\mathcal{D} \geq \lambda g$ which is non-negative. As a consequence, the second law of thermodynamics is indeed automatically ensured.

The model is closed by loading/unloading conditions. They can be defined by introducing a space of admissible stresses $\mathbb{E}_{\boldsymbol{\Sigma}}$. In line with the reduced dissipation inequality (6), this space is described in terms of $\boldsymbol{\Sigma}$ and $\boldsymbol{Q}$, i.e.,

$$\mathbb{E}_{\boldsymbol{\Sigma}} = \left\{ (\boldsymbol{\Sigma}, \boldsymbol{Q}) \in \mathbb{R}^{9+n} \;\middle|\; \phi(\boldsymbol{\Sigma}, \boldsymbol{Q}) \leq 0 \right\}. \tag{8}$$

According to Eq. (8), space $\mathbb{E}_{\boldsymbol{\Sigma}}$ is spanned by a function ϕ referred to as yield function. This function has to fulfill certain regularity conditions and is usually assumed to be convex. Based on the space of admissible stresses (8), the loading and unloading conditions can now be specified by

$$\lambda \, \phi = 0, \qquad \lambda \, \dot{\phi} = 0. \tag{9}$$

For (plastic) loading, $\lambda > 0$ and the plastic multiplier is computed from Eq. $(9)_2$, i.e., from the consistency condition $\dot{\phi} = 0$.

2.2. Prototype model

According to the general framework summarized in the previous subsection, a plasticity model can be defined by choosing a suitable Helmholtz energy Ψ, a plastic potential g (or several potentials) and a yield function ϕ. Regarding the latter, the Hill-type function

$$\phi := \sqrt{(\mathrm{dev}\boldsymbol{\Sigma} - \boldsymbol{Q}_{\mathrm{kin}}) : \mathbb{H} : (\mathrm{dev}\boldsymbol{\Sigma} - \boldsymbol{Q}_{\mathrm{kin}})} - Q_{\mathrm{iso}} - Q_0 \tag{10}$$

will be considered in what follows. Here, the stress-like internal variables $\boldsymbol{Q}$ have been split into a scalar-valued variable Q_{iso} capturing isotropic hardening and $\boldsymbol{Q}_{\mathrm{kin}}$ associated with kinematic hardening. Distortional hardening is excluded for now, but will be discussed in detail later. Thus, the fourth-order tensor $\mathbb{H}$ defining the material symmetry of the yield function is assumed as constant here. Clearly, although Eq. (10) represents quite a general framework, some important effects such as the strength differential effect are not covered. However, it bears emphasis that the distortional hardening models elaborated in the next sections can also be applied, if other yield functions are adopted.

The prototype model is completed by suitable hardening laws and by constituting the elastic response. For that purpose, a Helmholtz energy Ψ and a plastic potential g are required. Clearly, standard models can be used for isotropic hardening as well as for the elastic response. Within the examples presented in Section 4, an isotropic neo-Hooke model is employed for Ψ^{e} and isotropic hardening is captured by an exponentially saturating function. With respect to kinematic hardening, an

Armstrong-Frederick-type law is chosen. In summary, the prototype model is closed by the constitutive equations

$$\Psi = \Psi^{\mathrm{e}} + \Psi^{\mathrm{p}}_{\mathrm{iso}}(\alpha_{\mathrm{iso}}) + \Psi^{\mathrm{p}}_{\mathrm{kin}}(\boldsymbol{\alpha}_{\mathrm{kin}}), \qquad \Psi^{\mathrm{p}}_{\mathrm{kin}} = \frac{1}{2}\, c_{\mathrm{kin}}\, ||\boldsymbol{\alpha}_{\mathrm{kin}}||^2 \tag{11}$$

and

$$g = \phi + \frac{1}{2}\, \frac{b_{\mathrm{kin}}}{c_{\mathrm{kin}}}\, ||\boldsymbol{Q}_{\mathrm{kin}}||^2. \tag{12}$$

Here, c_{kin} and b_{kin} are model parameters.

Remark 1. *In order to guarantee saturation of the back stress tensor for any fourth-order tensor $\mathbb{H}$ (see Eq. (10)), a slightly modified Armstrong-Frederick model is adopted, cf. Feigenbaum and Dafalias (2007). In contrast to the model described before, it cannot be derived from a potential. However, it does fulfill the second law of thermodynamics. While Eq. (12) combined with Eq. (11) results in the evolution equation*

$$\dot{\boldsymbol{\alpha}}_{\mathrm{kin}} = \lambda(-\partial_{\boldsymbol{\Sigma}}\phi - b_{\mathrm{kin}}\boldsymbol{\alpha}_{\mathrm{kin}}) \tag{13}$$

the modification

$$\dot{\boldsymbol{\alpha}}_{\mathrm{kin}} = \lambda(-\partial_{\boldsymbol{\Sigma}}\phi - \|\partial_{\boldsymbol{\Sigma}}\phi\| b_{\mathrm{kin}}\boldsymbol{\alpha}_{\mathrm{kin}}) \quad \Rightarrow \quad \dot{\boldsymbol{Q}}_{\mathrm{kin}} = \lambda\|\partial_{\boldsymbol{\Sigma}}\phi\| \left(c_{\mathrm{kin}} \frac{\partial_{\boldsymbol{\Sigma}}\phi}{\|\partial_{\boldsymbol{\Sigma}}\phi\|} - b_{\mathrm{kin}}\boldsymbol{Q}_{\mathrm{kin}} \right) \tag{14}$$

was employed in Feigenbaum and Dafalias (2007). Accordingly, the back stress saturates to

$$\boldsymbol{Q}_{\mathrm{kin}} \overset{t\to\infty}{\to} \frac{c_{\mathrm{kin}}}{b_{\mathrm{kin}}} \frac{\partial_{\boldsymbol{\Sigma}}\phi}{\|\partial_{\boldsymbol{\Sigma}}\phi\|}. \tag{15}$$

3. Modeling of distortional hardening

So far, the shape of the yield function has been assumed as constant, i.e., only isotropic and kinematic hardening effects have been accounted for. In this section, extended models focusing on the shape change of the yield functions are presented.

3.1. Existing hardening models

In the paper Shi and Mosler (2013), some of the most frequently applied models dealing with distortional hardening are critically analyzed and compared to each other. It turns out that all of them share an important similarity: they model distortional hardening by means of an Armstrong-Frederick-type evolution equation. Inspired by the analogy to kinematic hardening, the Helmholtz energy

$$\Psi := \Psi^{\mathrm{e}} + \Psi^{\mathrm{p}}_{\mathrm{iso}} + \Psi^{\mathrm{p}}_{\mathrm{kin}} + \Psi^{\mathrm{p}}_{\mathrm{dis}}, \qquad \Psi^{\mathrm{p}}_{\mathrm{dis}} := \frac{1}{2}\, c_{\mathrm{dis}}\, \mathbb{E} :: \mathbb{E} \tag{16}$$

and the plastic potential

$$g := \phi + \frac{1}{2}\frac{b_{\mathrm{dis}}}{c_{\mathrm{dis}}}\, \mathbb{H} :: \mathbb{H} \tag{17}$$

are advocated in Shi and Mosler (2013) where $\mathbb{E}$ is energetically dual to $\mathbb{H}$, i.e., $\mathbb{H} := -\partial_{\mathbb{E}}\Psi$. Eqs. (16) and (17) imply the evolution equation

$$\dot{\mathbb{H}} = -\frac{c_{\mathrm{dis}}\lambda}{2}\frac{(\mathrm{dev}\boldsymbol{\Sigma} - \boldsymbol{Q}_{\mathrm{kin}}) \otimes (\mathrm{dev}\boldsymbol{\Sigma} - \boldsymbol{Q}_{\mathrm{kin}})}{\sqrt{(\mathrm{dev}\boldsymbol{\Sigma} - \boldsymbol{Q}_{\mathrm{kin}}) : \mathbb{H} : (\mathrm{dev}\boldsymbol{\Sigma} - \boldsymbol{Q}_{\mathrm{kin}})}} - b_{\mathrm{dis}}\lambda\mathbb{H}\,. \tag{18}$$

Although the results predicted by this evolution equation are indeed promising, Eq. (18) shows one drawback. This can be seen by considering radial loading paths. In this case, Eq. (18) leads to (if the differential equation converges)

$$\mathbb{H} \to -f\ (\mathrm{dev}\boldsymbol{\Sigma} - \boldsymbol{Q}_{\mathrm{kin}}) \otimes (\mathrm{dev}\boldsymbol{\Sigma} - \boldsymbol{Q}_{\mathrm{kin}}) \tag{19}$$

where $f \geq 0$ is a scalar not specified here. Consequently, all stress tensors being orthogonal to $\mathrm{dev}\boldsymbol{\Sigma} - \boldsymbol{Q}$ do not contribute to the equivalent stress

$$\Sigma^{\mathrm{eq}} = \sqrt{(\mathrm{dev}\boldsymbol{\Sigma} - \boldsymbol{Q}_{\mathrm{kin}}) : \mathbb{H} : (\mathrm{dev}\boldsymbol{\Sigma} - \boldsymbol{Q}_{\mathrm{kin}})}. \tag{20}$$

Hence, the admissible stress space is unbounded and non-physical stresses of infinite magnitude are possible. It bears emphasis that this problem is also present in other formulations, cf. Barthel et al. (2008); Noman et al. (2010).

The only model analyzed in Shi and Mosler (2013) which does not show the aforementioned problem is the one proposed by Feigenbaum & Dafalias, cf. Feigenbaum and Dafalias (2007). The underlying idea of this model is to decompose $\mathbb{H}$ into two parts, i.e.,

$$\mathbb{H} := \mathbb{H}_0 + \mathbb{A} \tag{21}$$

and to assign an evolution equation of the type (18) to the fourth-order tensor $\mathbb{A}$. While the constant tensor $\mathbb{H}_0$ is associated with the initial anisotropy, $\mathbb{A}$ captures the

effect of distortional hardening. Even if $\mathbb{A}$ converged to zero, the fourth-order tensor $\mathbb{H}$ entering the yield function could still be positive definite implying a bounded space of admissible stresses. However, a straightforward application of this modification creates another problem. If softening is to be modeled, $\mathbb{A}$ has to be positive definite, which would contradict Eq. (19). By replacing the + in the plastic potential (17) by −, this problem would certainly be eliminated. However, the second law of thermodynamics could then be violated. This dilemma can be solved by changing the sign of the term in Eq. (16) which is related to $\Psi^{\mathrm{p}}_{\mathrm{dis}}$, cf. Feigenbaum and Dafalias (2007). However, although a physical interpretation of this idea can be found in Feigenbaum and Dafalias (2007), this viewpoint is debatable from the authors' point of view.

3.2. A novel thermodynamically consistent model - dynamic hardening

The discussion presented in the previous subsection underlines the need for a new distortional hardening model that: (a) accounts for distortional hardening and (b) which exhibits a bounded space of admissible stresses. For the sake of simplicity, only hardening caused by currently active dislocations is considered, i.e., dynamic hardening, cf. Boers et al. (2010); Noman et al. (2010). The more general case will be elaborated in the next subsections.

Inspired by the decomposition of the Hill-type tensor $\mathbb{H}$ into one part due to the initial anisotropy $\mathbb{H}_0$ and an additional part related to its evolution $\mathbb{A}$, $\mathbb{H}$ is decomposed as (cf. Feigenbaum and Dafalias (2007))

$$\mathbb{H} = (1 - b_{\mathrm{D}})\mathbb{H}_0 + b_{\mathrm{D}}\mathbb{A}, \tag{22}$$

where b_{D} is a weighting coefficient (assumed as constant). Since this factor should not affect the material's initial anisotropy, the internal variable $\mathbb{A}$ is initialized as $\mathbb{A} = \mathbb{H}_0$. Assuming a quadratic Helmholtz energy $\Psi^{\mathrm{p}}_{\mathrm{dis}}$ of the type (16), the model is completed by suitable evolution equations. In order to fulfill the second law of thermodynamics, such equations are derived by means of the framework of generalized standard materials. Therefore, the only function which remains to be defined is the plastic potential g.

Focusing on dynamic hardening for now, hardening should be related to the current loading direction $\boldsymbol{N}$. In contrast to Shi and Mosler (2013) and in line with Feigenbaum and Dafalias (2007), this direction is approximated by means of the relative stresses. To be more precise, $\boldsymbol{N} := (\mathrm{dev}\boldsymbol{\Sigma} - \boldsymbol{Q}_{\mathrm{kin}})/\|\mathrm{dev}\boldsymbol{\Sigma} - \boldsymbol{Q}_{\mathrm{kin}}\|$. With this definition, an evolution equation of the type

$$\dot{\mathbb{E}} = \lambda\, h\, \boldsymbol{N} \otimes \boldsymbol{N} \tag{23}$$

characterizes dynamic hardening where h is a suitable scalar-valued variable. The probably simplest plastic potential corresponding to Eq. (23) is given by

$$g_{\text{dis}} = \frac{1}{2} \left(\boldsymbol{N} : \mathbb{A} : \boldsymbol{N} \right)^2 \geq 0. \tag{24}$$

It bears emphasis that the plastic potential (24) is not of typical Armstrong-Frederick-type as it does not involve the yield function. With the quadratic stored energy

$$\Psi^{\text{p}}_{\text{dis}} = \frac{1}{2} \, c_{\text{D}} \, \mathbb{E} :: \mathbb{E} \qquad \text{and} \qquad \mathbb{A} = -\partial_{\mathbb{E}} \Psi \tag{25}$$

the plastic potential (24) yields the evolution equation

$$\dot{\mathbb{A}} = -c_{\text{D}} \dot{\mathbb{E}} = -c_{\text{D}} \lambda \left(\boldsymbol{N} : \mathbb{A} : \boldsymbol{N} \right) \boldsymbol{N} \otimes \boldsymbol{N}. \tag{26}$$

Here, c_{D} is a model parameter related to distortional hardening. Adopting associative evolution equations for the flow rule and for isotropic hardening, the Armstrong-Frederick-law (11) and (12) for kinematic hardening and Eqs. (25) and (26) for distortional hardening, a lengthy, but nevertheless straightforward calculation, yields

$$\mathcal{D} = \lambda Q_0 + \lambda (\boldsymbol{N} : \mathbb{A} : \boldsymbol{N})^2 + \lambda \, b_{\text{kin}} \, c_{\text{kin}} \| \partial_{\boldsymbol{\Sigma}} \phi \| \| \boldsymbol{\alpha}_{\text{kin}} \|^2 \geq 0. \tag{27}$$

Consequently, and in line with the convexity of the non-negative plastic potentials, the second law of thermodynamics is indeed fulfilled (if $b_{\text{kin}} \geq 0$ and $c_{\text{kin}} \geq 0$).

Remark 2. *The evolution equation (26) indeed converges and the resulting fourth-order tensor $\mathbb{H}$ defines an admissible stress space in which all stresses are bounded, cf. Subsection 3.4.2.*

3.3. A novel thermodynamically consistent model – dynamic and latent hardening

According to Barthel et al. (2008); Noman et al. (2010); Shi and Mosler (2013), one evolution equation of the type (18) or (26) is usually not flexible enough to model the hardening response of real materials. A possible improvement can be realized by decomposing the total hardening behavior into latent and dynamic parts, cf. Noman et al. (2010); Haddadi et al. (2006). Extending the decomposition (22) within this respect yields

$$\mathbb{H} = \left[1 - b_{\text{D}} - b_{\text{L}} \right] \mathbb{H}_0 + b_{\text{D}} \, \mathbb{A}_{\text{D}} + b_{\text{L}} \, \mathbb{A}_{\text{L}} \, . \tag{28}$$

Here, b_{D} and b_{L} are weighting parameters related to dynamic and latent hardening. By choosing the initial values as $\mathbb{A}_{\text{D}} = \mathbb{H}_0$ and $\mathbb{A}_{\text{L}} = \mathbb{H}_0$, the weighting parameters do not influence the intial yield surface. A similar decomposition of distortional

hardening can also be found in (Haddadi et al., 2006; Hiwatashi et al., 1998; Wang et al., 2008). However, thermodynamical consistency of these models is not clear – at least, it has not been checked.

By decomposing the fourth-order identity tensor $\mathbb{I}^{\mathrm{dev}}$ into the dynamic part $\boldsymbol{N} \otimes \boldsymbol{N}$ and into the orthogonal direction $\mathbb{I}^{\mathrm{dev}} - \boldsymbol{N} \otimes \boldsymbol{N}$, the canonical extension of the plastic potential (24) reads

$$g_{\mathrm{dis}} = \frac{1}{2}(\boldsymbol{N} : \mathbb{A}_{\mathrm{D}} : \boldsymbol{N})^2 + \frac{1}{2}\big[\big(\mathbb{I}^{\mathrm{dev}} - \boldsymbol{N} \otimes \boldsymbol{N}\big) :: \mathbb{A}_{\mathrm{L}}\big]^2. \tag{29}$$

Thus, with the quadratic parts

$$\Psi^{\mathrm{p}}_{\mathrm{dis}} = \Psi^{\mathrm{p}}_{\mathrm{dis,D}} + \Psi^{\mathrm{p}}_{\mathrm{dis,L}}, \quad \Psi^{\mathrm{p}}_{\mathrm{dis,D}} = \frac{1}{2}\, c_{\mathrm{D}}\, \mathbb{E}_{\mathrm{D}} :: \mathbb{E}_{\mathrm{D}}, \quad \Psi^{\mathrm{p}}_{\mathrm{dis,L}} = \frac{1}{2}\, c_{\mathrm{L}}\, \mathbb{E}_{\mathrm{L}} :: \mathbb{E}_{\mathrm{L}} \tag{30}$$

of the stored Hemholtz energy, the resulting evolution equations are given by

$$\dot{\mathbb{A}}_{\mathrm{D}} = -c_{\mathrm{D}}\dot{\mathbb{E}}_{\mathrm{D}} = -c_{\mathrm{D}}\lambda\,(\boldsymbol{N} : \mathbb{A}_{\mathrm{D}} : \boldsymbol{N})\,\boldsymbol{N} \otimes \boldsymbol{N} \tag{31}$$

$$\dot{\mathbb{A}}_{\mathrm{L}} = -c_{\mathrm{L}}\dot{\mathbb{E}}_{\mathrm{L}} = -c_{\mathrm{L}}\lambda\,\big[\big(\mathbb{I}^{\mathrm{dev}} - \boldsymbol{N} \otimes \boldsymbol{N}\big) :: \mathbb{A}_{\mathrm{L}}\big]\,\big(\mathbb{I}^{\mathrm{dev}} - \boldsymbol{N} \otimes \boldsymbol{N}\big). \tag{32}$$

In line with the model presented before, c_{D} and c_{L} are model parameters related to dynamic and latent distortional hardening. Accordingly, dynamic hardening is always associated with the current loading direction $\boldsymbol{N} \otimes \boldsymbol{N}$, while latent hardening corresponds to the orthogonal directions $\mathbb{I}^{\mathrm{dev}} - \boldsymbol{N} \otimes \boldsymbol{N}$. The previous models proposed in Barthel et al. (2008); Noman et al. (2010) do not show such a disjunct decomposition. Again, adopting associative evolution equations for the flow rule and for isotropic hardening, the Armstrong-Frederick-law (11) and (12) for kinematic hardening and Eqs. (29) and (30) for distortional hardening, a lengthy, but nevertheless straightforward calculation, yields

$$\begin{aligned} \mathcal{D} \;=\; & \lambda Q_0 + \lambda(\boldsymbol{N} : \mathbb{A}_{\mathrm{D}} : \boldsymbol{N})^2 + \lambda\big[\big(\mathbb{I}^{\mathrm{dev}} - \boldsymbol{N} \otimes \boldsymbol{N}\big) :: \mathbb{A}_{\mathrm{L}}\big]^2 \\ & + \lambda\, b_{\mathrm{kin}}\, c_{\mathrm{kin}} \|\partial_{\boldsymbol{\Sigma}}\phi\| \|\boldsymbol{\alpha}_{\mathrm{kin}}\|^2 \geq 0. \end{aligned} \tag{33}$$

According to Eq. (33) and independent of the material parameters ($b_{\mathrm{kin}} \geq 0, c_{\mathrm{kin}} \geq 0$), the dissipation is indeed non-negative and the second law of thermodynamics is thus fulfilled.

Remark 3. *The evolution equations (31) and (32) indeed converge and the resulting fourth-order tensor $\mathbb{H}$ defines an admissible stress space in which all stresses are bounded, cf. Subsection 3.4.2.*

3.4. A novel thermodynamically consistent model – dynamic/latent hardening and higher curvature in loading direction

3.4.1. Fundamentals

To the best knowledge of the authors, the model elaborated in the previous subsection is the first one which accounts for dynamic and latent hardening and for which thermodynamical consistency has been explicitly proven. In its present form, it can already be applied to a broad variety of different alloys. However, some alloys such as high-strength aluminum alloys show a higher curvature of the yield function in loading direction compared to the opposite reverse direction. This suggests a further decomposition of dynamic hardening according to these directions. A first model for this was proposed in Feigenbaum and Dafalias (2007). In this model, the current loading direction is approximated by the normalized relative stresses $\boldsymbol{N}$, while the previous loading direction (history) is captured by the back stresses $\boldsymbol{Q}_{\mathrm{kin}}$. Consequently, the scalar product $\boldsymbol{N} : \boldsymbol{Q}_{\mathrm{kin}}$ attains its maximum, if $\boldsymbol{N}$ and $\boldsymbol{Q}_{\mathrm{kin}}$ point into the same direction, while its minimum is associated with the negative normalized stress $-\boldsymbol{N}$.

The just described idea proposed in Feigenbaum and Dafalias (2007) can be incorporated into the current framework in a straightforward manner. For this purpose, the Hill-type tensor $\mathbb{H}$ is further decomposed, i.e.

$$\mathbb{H} = \left[1 - b_{\mathrm{D}} - b_{\mathrm{C}}(\boldsymbol{N} : \boldsymbol{Q}_{\mathrm{kin}}) - b_{\mathrm{L}}\right] \mathbb{H}_0 + \left[b_{\mathrm{D}} + b_{\mathrm{C}}(\boldsymbol{N} : \boldsymbol{Q}_{\mathrm{kin}})\right] \mathbb{A}_{\mathrm{D}} + b_{\mathrm{L}} \mathbb{A}_{\mathrm{L}}. \tag{34}$$

While the model parameters b_{D} and b_{L} are related to the dynamic and latent hardening as discussed in the previous subsection, the new parameter b_{C} controls the curvature difference in the loading direction and in the reverse direction. It therefore corresponds to dynamic hardening (loading direction).

It bears emphasis that the introduction of the additional term $b_{\mathrm{C}}(\boldsymbol{N} : \boldsymbol{Q}_{\mathrm{kin}})$ in Eq. (34) is the only modification necessary in order to model a different curvature of the yield surface in the loading and the opposite direction. All other constitutive equations are those discussed in the previous subsection. Accordingly, the evolution equations are not changed at all, rendering the dissipation inequality

$$\begin{aligned} \mathcal{D} \;=\; & \lambda Q_0 + \lambda (\boldsymbol{N} : \mathbb{A}_{\mathrm{D}} : \boldsymbol{N})^2 + \lambda \left[\left(\mathbb{I}^{\mathrm{dev}} - \boldsymbol{N} \otimes \boldsymbol{N} \right) :: \mathbb{A}_{\mathrm{L}} \right]^2 \\ & + \lambda \; b_{\mathrm{kin}} \; c_{\mathrm{kin}} \| \partial_{\boldsymbol{\Sigma}} \phi \| \| \boldsymbol{\alpha}_{\mathrm{kin}} \|^2 \geq 0 \end{aligned} \tag{35}$$

to be identical to the one in the model presented in the previous subsection (cf. to Eq. (33)). As a result, the second law of thermodynamics is still fulfilled.

The generalized model for distortional hardening is summarized in the Tab. 1.

- Helmholtz energy

$$\Psi = \Psi^{\mathrm{e}}(\boldsymbol{F}^{\mathrm{e}}) + \Psi^{\mathrm{p}}_{\mathrm{iso}}(\alpha_{\mathrm{iso}}) + \Psi^{\mathrm{p}}_{\mathrm{kin}}(\boldsymbol{\alpha}_{\mathrm{kin}}) + \Psi^{\mathrm{p}}_{\mathrm{disD}}(\mathbb{E}_{\mathrm{D}}) + \Psi^{\mathrm{p}}_{\mathrm{disL}}(\mathbb{E}_{\mathrm{L}}) \tag{36}$$

Hardening models

$$\begin{aligned}
&\Psi^{\mathrm{p}}_{\mathrm{iso}}(\alpha_{\mathrm{iso}}) = Q^{\infty}_{\mathrm{iso}} \left(\alpha_{\mathrm{iso}} + \tfrac{1}{c_{\mathrm{iso}}} \exp[-c_{\mathrm{iso}}\,\alpha_{\mathrm{iso}}]\right) && Q_{\mathrm{iso}} = -\partial_{\alpha_{\mathrm{iso}}}\Psi \\
&\Psi^{\mathrm{p}}_{\mathrm{kin}}(\boldsymbol{\alpha}_{\mathrm{kin}}) = \frac{1}{2}\, c_{\mathrm{kin}}\, ||\boldsymbol{\alpha}_{\mathrm{kin}}||^2 && \boldsymbol{Q}_{\mathrm{kin}} = -\partial_{\boldsymbol{\alpha}_{\mathrm{kin}}}\Psi \\
&\Psi^{\mathrm{p}}_{\mathrm{disD}}(\mathbb{E}_{\mathrm{D}}) = \frac{1}{2}\, c_{\mathrm{D}}\, ||\mathbb{E}_{\mathrm{D}}||^2 && \mathbb{A}_{\mathrm{D}} = -\partial_{\mathbb{E}_{\mathrm{D}}}\Psi \\
&\Psi^{\mathrm{p}}_{\mathrm{disL}}(\mathbb{E}_{\mathrm{L}}) = \frac{1}{2}\, c_{\mathrm{L}}\, ||\mathbb{E}_{\mathrm{L}}||^2 && \mathbb{A}_{\mathrm{L}} = -\partial_{\mathbb{E}_{\mathrm{L}}}\Psi
\end{aligned} \tag{37}$$

- Yield function ϕ and decomposition of the Hill-type tensor $\mathbb{H}$

$$\phi := \sqrt{(\mathrm{dev}\boldsymbol{\Sigma} - \boldsymbol{Q}_{\mathrm{kin}}) : \mathbb{H} : (\mathrm{dev}\boldsymbol{\Sigma} - \boldsymbol{Q}_{\mathrm{kin}})} - Q_{\mathrm{iso}} - Q_0 \tag{38}$$

$$\begin{aligned}
\mathbb{H} = {} & [1 - b_{\mathrm{D}} - b_{\mathrm{C}}(\boldsymbol{N} : \boldsymbol{Q}_{\mathrm{kin}}) - b_{\mathrm{L}}]\, \mathbb{H}_0 \\
& + [b_{\mathrm{D}} + b_{\mathrm{C}}(\boldsymbol{N} : \boldsymbol{Q}_{\mathrm{kin}})]\, \mathbb{A}_{\mathrm{D}} + b_{\mathrm{L}}\mathbb{A}_{\mathrm{L}}
\end{aligned} \tag{39}$$

- Plastic potential for distortional hardening g_{dis}

$$g_{\mathrm{dis}} = \left\{ \frac{1}{2}(\boldsymbol{N} : \mathbb{A}_{\mathrm{D}} : \boldsymbol{N})^2 + \frac{1}{2}\left[\left(\mathbb{I}^{\mathrm{dev}} - \boldsymbol{N} \otimes \boldsymbol{N}\right) :: \mathbb{A}_{\mathrm{L}}\right]^2 \right\}\, h_{\mathrm{u}} \tag{40}$$

- Evolution equations (generalized standard materials)

$$\dot{\alpha}_{\mathrm{iso}} = -\lambda \tag{41}$$

$$\dot{\boldsymbol{\alpha}}_{\mathrm{kin}} = \lambda \|\partial_{\boldsymbol{\Sigma}}\phi\| \left(-\frac{\partial_{\boldsymbol{\Sigma}}\phi}{\|\partial_{\boldsymbol{\Sigma}}\phi\|} - b_{\mathrm{kin}}\boldsymbol{\alpha}_{\mathrm{kin}} \right) \tag{42}$$

$$\dot{\mathbb{E}}_{\mathrm{D}} = -\left\{ c_{\mathrm{D}}\, \lambda\, (\boldsymbol{N} : \mathbb{E}_{\mathrm{D}} : \boldsymbol{N})\, \boldsymbol{N} \otimes \boldsymbol{N} \right\}\, h_{\mathrm{u}} \tag{43}$$

$$\dot{\mathbb{E}}_{\mathrm{L}} = -\left\{ c_{\mathrm{L}}\, \lambda \left[\left(\mathbb{I}^{\mathrm{dev}} - \boldsymbol{N} \otimes \boldsymbol{N}\right) :: \mathbb{E}_{\mathrm{L}}\right] \left(\mathbb{I}^{\mathrm{dev}} - \boldsymbol{N} \otimes \boldsymbol{N}\right) \right\}\, h_{\mathrm{u}} \tag{44}$$

Table 1: Summary of the generalized plasticity model. In contrast to the model described before, an additional factor $h_{\mathrm{u}} = 1$ MPa has been introduced in Eq. (40). This factor is not a material parameter, but just used in order to avoid inconsistencies regarding the physical units.

Remark 4. *The factor* $\mathbf{N} : \mathbf{Q}_{\mathrm{kin}}$ *governing the curvature difference is continuous in time. By way of contrast, the alternative factor* $\mathbf{N} : \mathbf{Q}_{\mathrm{kin}}/\|\mathbf{Q}_{\mathrm{kin}}\|$ *considered in Pietryga et al. (2012) is usually discontinuous in time. For instance, if the initial yield surface is of von Mises type and uniaxial loading followed by reverse loading is considered,* $\mathbf{N} : \mathbf{Q}_{\mathrm{kin}}/\|\mathbf{Q}_{\mathrm{kin}}\| \in \{-1; 1\}$*. Such a jump is questionable from a physics point of view and causes numerical problems.*

Remark 5. *According to Eq.*(34)*, the fourth-order tensor* $\mathbb{H}$ *shows major symmetry (in cartesian bases* $\mathbb{H}_{ijkl} = \mathbb{H}_{klij}$*) and is also deviatoric (in cartesian bases* $\mathbb{H}_{ijkk} = 0_{ij}$*).*

Remark 6. *Within the present framework, latent hardening is modeled in an isotropic fashion. To be more precise, any direction orthogonal to the current loading direction* $\boldsymbol{N} \otimes \boldsymbol{N}$ *shows the same response. Although the predictive capabilities of the model are promising, as demonstrated in the next section, the current latent hardening model might represent a too crude approximation for strongly anisotropic materials. In this case, the latent part* $\mathbb{I}^{\mathrm{dev}} - \boldsymbol{N} \otimes \boldsymbol{N}$ *could be further decomposed according to the axes of material symmetry.*

Remark 7. *The constitutive models elaborated here and in the previous subsections have been implemented by a currently standard return-mapping algorithm, cf. Simo (1998); Simo and Hughes (1998). For that purpose, the flow rule has been integrated by means of the exponential map, while the remaining evolution equations have been approximated in time by a backward-Euler integration.*

3.4.2. Convexity of the yield function - restrictions on material parameters

Starting from a convex initial yield function, the proposed framework does not guarantee the final yield function to still be convex. In this section, simple constraints for the model parameters guaranteeing convexity will be elaborated.

Saturation of the fourth-order tensor $\mathbb{H}$*.* In the following, it is shown first that the yield function indeed converges to a limiting yield surface. For that purpose, an arbitrary loading path is approximated by piece wise radial loading paths. If the respective radial loading direction (normalized relative stress) is given by $\boldsymbol{N}$, the evolution equation corresponding to dynamic hardening reads (cf. Eq. (26)),

$$\dot{\mathbb{A}}_{\mathrm{D}} = -\lambda c_{\mathrm{D}} (\boldsymbol{N} \otimes \boldsymbol{N} \otimes \boldsymbol{N} \otimes \boldsymbol{N}) :: \mathbb{A}_{\mathrm{D}} \tag{45}$$

with the analytical solution

$$\mathbb{A}_{\mathrm{D}}(t) = \exp[-\Delta\lambda_t c_{\mathrm{D}} (\boldsymbol{N} \otimes \boldsymbol{N} \otimes \boldsymbol{N} \otimes \boldsymbol{N})] :: \mathbb{A}_{\mathrm{D}0} \tag{46}$$

where $\mathbb{A}_{\mathrm{D}0}$ represents the initial state of $\mathbb{A}_{\mathrm{D}}$ and $\Delta\lambda_t$ is the integrated plastic multiplier. By a standard series expansion, the identity

$$\begin{aligned} & \exp[-\Delta\lambda_t c_{\mathrm{D}}(\boldsymbol{N}\otimes\boldsymbol{N}\otimes\boldsymbol{N}\otimes\boldsymbol{N})] \\ = \quad & \overset{(8)}{\mathbb{I}} + [\exp(-\Delta\lambda_t c_{\mathrm{D}}) - 1]\,(\boldsymbol{N}\otimes\boldsymbol{N}\otimes\boldsymbol{N}\otimes\boldsymbol{N})) \end{aligned} \tag{47}$$

is obtained with $\overset{(8)}{\mathbb{I}}$ denoting the eighth-order identity tensor. Inserting this series expansion into Eq. (46) and taking into account that $c_{\mathrm{D}} \geq 0$ eventually yields

$$\mathbb{A}_{\mathrm{D}}(t) \overset{t\to\infty}{\to} \mathbb{A}_{\mathrm{D}0} - (\boldsymbol{N} : \mathbb{A}_{\mathrm{D}0} : \boldsymbol{N})\boldsymbol{N}\otimes\boldsymbol{N}. \tag{48}$$

As a result, $\mathbb{A}_{\mathrm{D}}$ indeed converges (if $c_{\mathrm{D}} \geq 0$). Analogously, it can be shown that latent hardening converges to (if $c_{\mathrm{L}} \geq 0$)

$$\mathbb{A}_{\mathrm{L}}(t) \overset{t\to\infty}{\to} \mathbb{A}_{\mathrm{L}0} - \frac{1}{7}\left[(\mathbb{I}^{\mathrm{dev}} - \boldsymbol{N}\otimes\boldsymbol{N})\otimes(\mathbb{I}^{\mathrm{dev}} - \boldsymbol{N}\otimes\boldsymbol{N})\right] :: \mathbb{A}_{\mathrm{L}0} \tag{49}$$

and that the fourth-order tensor $\mathbb{H}$ according to Eq. (34) thus saturates (the back stress tensor also saturates, cf. Remark 1).

Remark 8. *If the initial values* $\mathbb{A}_{\mathrm{D}0} = \mathbb{A}_{\mathrm{L}0} = \mathbb{H}_0 = \mathbb{I}^{\mathrm{dev}}$ *are chosen, together with* $b_{\mathrm{D}} = b_{\mathrm{L}}$ *and* $c_{\mathrm{D}} = 7\,c_{\mathrm{L}}$*, the fourth-order tensor* $\mathbb{H}$ *in Eq.* (28) *reduces to*

$$\mathbb{H} = (1 - b_{\mathrm{D}} + b_{\mathrm{D}}\,\exp(-\Delta\lambda_t c_{\mathrm{D}}))\;\mathbb{I}^{\mathrm{dev}}\,. \tag{50}$$

According to Eq. (50), the distortional hardening model is then equivalent to isotropic hardening.

Convexity of the saturated yield function. Proving convexity of the yield function for arbitrary fourth-order tensors $\mathbb{A}_{\mathrm{D}0}$ and $\mathbb{A}_{\mathrm{L}0}$ is relatively difficult – it is at least difficult to derive simple constraints for the model parameters guaranteeing convexity. For this reason, focus here is on the model used in the numerical examples. Within this model, the initial yield surface is characterized by a von Mises yield function $\mathbb{H}_0 = \mathbb{A}_{\mathrm{D}0} = \mathbb{A}_{\mathrm{L}0} = \mathbb{I}^{\mathrm{dev}}$. In this case, the first radial-loading path leads to the saturated fourth-order tensor

$$\mathbb{H} = \mathbb{I}^{\mathrm{dev}} - \left(b_{\mathrm{D}} + b_{\mathrm{C}}\,\frac{c_{\mathrm{kin}}}{b_{\mathrm{kin}}}\,\alpha\right)\,\boldsymbol{N}\otimes\boldsymbol{N} - b_{\mathrm{L}}\,\left(\mathbb{I}^{\mathrm{dev}} - \boldsymbol{N}\otimes\boldsymbol{N}\right), \tag{51}$$

cf. Eq. (34). In Eq. (51), the saturated back stress

$$\boldsymbol{Q}_{\mathrm{kin}} \overset{t\to\infty}{\to} \frac{c_{\mathrm{kin}}}{b_{\mathrm{kin}}}\,\frac{\partial_{\boldsymbol{\Sigma}}\Sigma^{\mathrm{eq}}}{\|\partial_{\boldsymbol{\Sigma}}\Sigma^{\mathrm{eq}}\|} = \frac{c_{\mathrm{kin}}}{b_{\mathrm{kin}}}\,\boldsymbol{N}_{\phi}, \quad \boldsymbol{N}_{\phi} := \frac{\partial_{\boldsymbol{\Sigma}}\Sigma^{\mathrm{eq}}}{\|\partial_{\boldsymbol{\Sigma}}\Sigma^{\mathrm{eq}}\|}, \tag{52}$$

together with the abbreviation $\alpha := \boldsymbol{N} : \boldsymbol{N}_\phi$, has been inserted.

Based on Eq. (52) convexity can be analyzed. For that purpose, the respective condition

$$\boldsymbol{V} : \frac{\partial^2 \phi}{\partial \boldsymbol{\Sigma}^2} : \boldsymbol{V} \geq 0 \qquad \forall \boldsymbol{V} \tag{53}$$

is computed. Here and in the following, $\boldsymbol{V}$ is an arbitrary normalized deviatoric second-order tensor. After a lengthy but straightforward calculation, Ineq. (53) can be rewritten as

$$\begin{aligned} & \|\mathrm{dev}\boldsymbol{\Sigma} - \boldsymbol{Q}_{\mathrm{kin}}\| \, \boldsymbol{V} : \frac{\partial^2 \phi}{\partial \boldsymbol{\Sigma}^2} : \boldsymbol{V} \qquad (54) \\ = \; & \frac{1}{\sqrt{1 - b_{\mathrm{D}} - b_{\mathrm{C}} \frac{c_{\mathrm{kin}}}{b_{\mathrm{kin}}} \alpha}} \Bigg\{ 1 + \frac{b_{\mathrm{C}}}{2} \frac{c_{\mathrm{kin}}}{b_{\mathrm{kin}}} \alpha - \left(b_{\mathrm{D}} + \frac{b_{\mathrm{C}}}{2} \frac{c_{\mathrm{kin}}}{b_{\mathrm{kin}}} \alpha \right) \beta^2 \\ & - b_{\mathrm{L}} \left(1 - \beta^2 \right) - b_{\mathrm{C}} \frac{c_{\mathrm{kin}}}{b_{\mathrm{kin}}} \beta \gamma - \frac{\left[\left(1 - b_{\mathrm{D}} - \frac{b_{\mathrm{C}}}{2} \frac{c_{\mathrm{kin}}}{b_{\mathrm{kin}}} \alpha \right) \beta - \frac{b_{\mathrm{C}}}{2} \frac{c_{\mathrm{kin}}}{b_{\mathrm{kin}}} \gamma \right]^2}{1 - b_{\mathrm{D}} - b_{\mathrm{C}} \frac{c_{\mathrm{kin}}}{b_{\mathrm{kin}}} \alpha} \Bigg\} \geq 0 \end{aligned}$$

where $\beta := \boldsymbol{V} : \boldsymbol{N}$ and $\gamma := \boldsymbol{V} : \boldsymbol{N}_\phi$.

If the curvature difference of the yield function in loading and the opposite direction is neglected ($b_{\mathrm{C}} = 0$), Ineq. (54) can be significantly simplified. To be more precise, convexity of the yield function requires in this case

$$\|\mathrm{dev}\boldsymbol{\Sigma} - \boldsymbol{Q}_{\mathrm{kin}}\| \, \boldsymbol{V} : \frac{\partial^2 \phi}{\partial \boldsymbol{\Sigma}^2} : \boldsymbol{V} = \frac{(1 - \beta^2)(1 - b_{\mathrm{L}})}{\sqrt{1 - b_{\mathrm{D}}}} \geq 0. \tag{55}$$

Since $\beta = \boldsymbol{V} : \boldsymbol{N} \in [-1, +1]$ implying $(1 - \beta^2) \geq 0$, two conditions have to be fulfilled in order to guarantee Ineq. (55). They are:

$$b_{\mathrm{D}} < 1, \quad b_{\mathrm{L}} < 1, \tag{56}$$

These conditions are fulfilled for all models presented in Section 4.

With respect to the fully coupled model, also showing a different curvature of the yield function in loading direction and the opposite direction, simple conditions such as those in Ineq. (56) could not be derived. However, according to Ineq. (54), a simple necessary condition for convexity is

$$1 - b_{\mathrm{D}} - b_{\mathrm{C}} \frac{c_{\mathrm{kin}}}{b_{\mathrm{kin}}} \alpha > 0. \tag{57}$$

It can be shown that this condition is equivalent to

$$\boldsymbol{V} : \mathbb{H} : \boldsymbol{V} \geq 0 \qquad \forall \boldsymbol{V}. \tag{58}$$

Since $b_{\mathrm{C}} \geq 0$ and $c_{\mathrm{kin}}/b_{\mathrm{kin}} \geq 0$, Ineq. (57) is fulfilled, if (sufficient condition)

$$1 - b_{\mathrm{D}} - b_{\mathrm{C}} \frac{c_{\mathrm{kin}}}{b_{\mathrm{kin}}} > 0. \tag{59}$$

This constraint is fulfilled by all models in Section 4.

Remark 9. *In the present section, necessary and sufficient conditions for guaranteeing convexity of the limiting yield surface including dynamic and latent hardening have been derived. Regarding the model which also captures a different curvature of the yield surface in the loading and in the unloading direction, only necessary conditions have been elaborated. An important step towards the derivation of sufficient conditions would be a relation between* $\beta := \boldsymbol{V} : \boldsymbol{N}$ *and* $\gamma := \boldsymbol{V} : \boldsymbol{N}_{\phi}$*. In Plesek et al. (2010), the relation*

$$\boldsymbol{N} : \boldsymbol{N}_{\phi} = cos(\beta \pm \gamma) \tag{60}$$

with

$$\cos\beta = \boldsymbol{V} : \boldsymbol{N}, \qquad \cos\gamma = \boldsymbol{V} : \boldsymbol{N}_{\phi} \tag{61}$$

was used ($\boldsymbol{V}$ *is still an arbitrary normalized deviatoric second-order tensor). However, this relation is usually not fulfilled and can therefore only hold under certain constitutive assumptions.*

4. Predictive capabilities of the novel model

The predictive capabilities of the novel models are shown here by computing the evolution of yield surfaces for different materials and comparing these surfaces to their experimentally measured counterparts. The material parameters of the models have been identified by means of a standard least squares fit, i.e., minimization of the difference between all experimentally measured yield surfaces for a certain material and those surfaces predicted from the model. For the initial yield surface, an isotropic yield surface is assumed, i.e., $\mathbb{H}_0 = \mathbb{A}_{\mathrm{D}0} = \mathbb{A}_{\mathrm{L}0} = \mathbb{I}^{\mathrm{dev}}$. A summary of the material parameters is given in the appendix of this paper.

4.1. Aluminum alloy Al6061-T6511

According to the experimental measurements reported in Khan et al. (2009), aluminum alloy Al6061-T6511 shows a pronounced distortion of the yield surface during deformation. Furthermore, the respective yield loci have a higher curvature in loading direction compared to the opposite reverse direction. Within the experiments reported in Khan et al. (2009), a bar made of Al6061-T6511 is deformed under monotonic uniaxial tension (strain-controlled). The results of the novel model together with their experimentally measured counterparts are given in Fig. 2. Three yield surfaces corresponding to engineering strains of 2%, 4% and 6% are summarized in this figure. As can be seen, the surfaces predicted by the novel model are in excellent agreement with the experimental measurements. All characteristic features of the investigated aluminium alloy Al6061-T6511 are captured such as high curvature changes of the yield surface as well as an exceeding dynamic and latent softening.

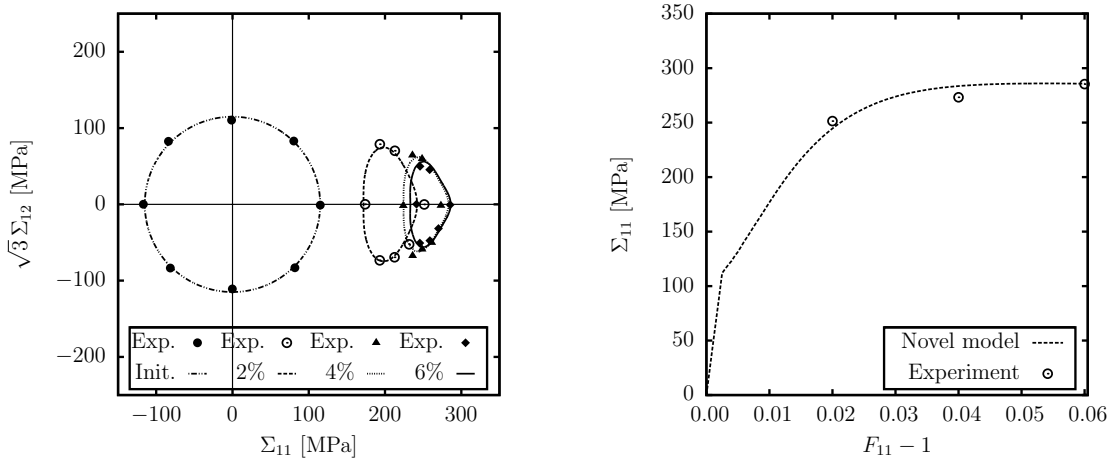

Figure 2: Evolution of the yield surface (left) for aluminum alloy 6061-T6511 subjected to simple tension of 2%, 4% and 6%. The respective stress-strain response is shown in the right diagram. Lines represent the predictions obtained from the novel model, while the symbols are associated with the experimental measurements reported in Khan et al. (2009).

4.2. Aluminum alloy AU4G T4 (2024)

Aluminium alloy AU4G T4 (2024) is investigated next. According to the experimental measurements in M. Boucher (1995), this alloy shows a similar mechanical response as does Al6061-T6511. However, the experiments conducted in M. Boucher (1995) are based on a combined tension/shear test. To be more precise, the material is first loaded in pure tension, followed by unloading to 100 MPa and subsequently

deformed under torsion. Comparison of the model predictions with the results obtained from the experiments in M. Boucher (1995) are depicted in Fig. 3. Again, the model captures all characteristic mechanical features of the considered alloy well: high curvature changes of the yield surface as well as pronounced dynamic and latent hardening. For the sake of comparison, predictions obtained from the model proposed in Feigenbaum and Dafalias (2007); Plesek et al. (2010) are also given in Fig. 3. By comparing the yield surfaces it can be seen that only the novel model allows capturing of the cross hardening effect. The model as advocated in Feigenbaum and Dafalias (2007); Plesek et al. (2010) yields a maximum stress $\sqrt{2}\Sigma_{12}$ which remains almost constant during the first loading regime (Fig. 3 (b)).

4.3. Stainless steel SUS304

Finally, the stainless steel SUS304 is analyzed. Although the experiments described in Ishikawa (1997) confirm a distortion of the yield surface, this surface has the same curvature in loading and in the opposite reverse direction. For this reason, the model parameter b_{C} can be set to zero. The computed evolution of the yield surfaces is summarized in Fig. 4. The underlying loading path is similar to that of the aluminum alloy AU4G T4 (2024), i.e., a simple tension test is followed by torsion. For the sake of comparison, predictions obtained from the model (Dafalias et al., 2003; Schick, 2004) are also included in Fig. 4. While for the novel model, the parameters corresponding to the initial yield surface have been computed first and fixed during the identification procedure related to distortional hardening, that seems not to be the case within the results published in Dafalias et al. (2003); Schick (2004) (Fig. 4 (a)). During the first loading regime in Fig. 4 (b), the agreement between the computations of the novel model and the experimental measurements is excellent. When the loading direction is changed the agreement is still good. In the second loading phase (torsion), the yield surface rotates (Fig. 4(c)). The predicted yield surface of the novel model seems to be more realistic than the counterpart corresponding to the model proposed in Dafalias et al. (2003); Schick (2004). In summary, the novel model captures also the most relevant hardening mechanisms for the stainless steel SUS304.

5. Conclusion

In this paper, a novel constitutive model suitable for distortional hardening was presented. To the best knowledge of the authors, this model is the first one which combines the following features: (1) proof of thermodynamical consistency (2) decomposition of hardening into dynamic and latent hardening (3) difference of the

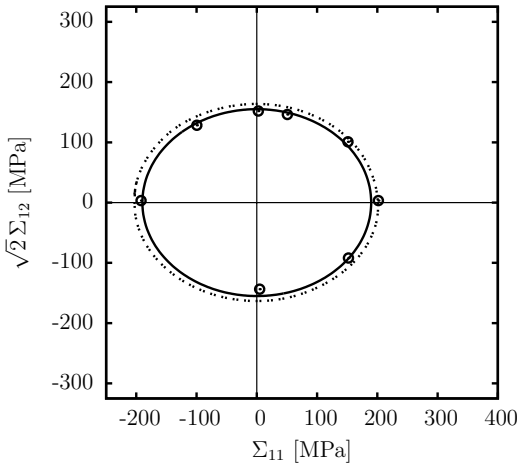

(a) Initial yield surface

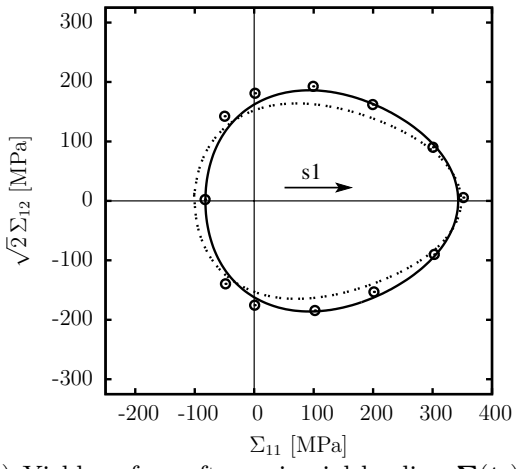

(b) Yield surface after uni-axial loading $\boldsymbol{\Sigma}(t_1) = \Sigma_{11}(t_1)\,\mathbf{e}_1 \otimes \mathbf{e}_1$

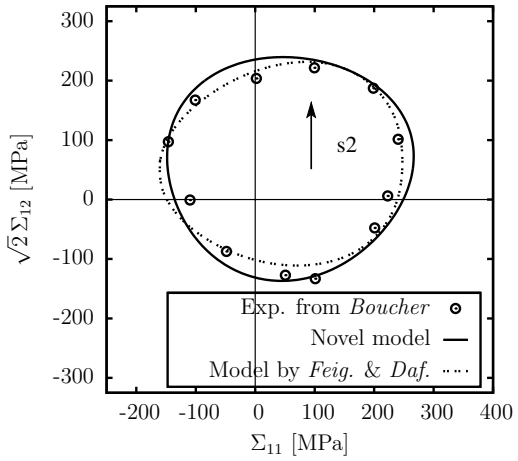

(c) Yield surface after tension unloading to 100 [MPa] and subsequent torsional loading $\boldsymbol{\Sigma}(t_2) = 100\ \text{MPa}\,\mathbf{e}_1 \otimes \mathbf{e}_1 + \Sigma_{12}(t_2)\,\text{sym}(\mathbf{e}_1 \otimes \mathbf{e}_2)$

Figure 3: Evolution of the yield surface for the aluminum alloy AU4G T4 (2024) subjected to simple tension, followed by torsion. Novel model: solid line. Model proposed in Feigenbaum and Dafalias (2007): dashed line. The symbols are associated with the experimental measurements reported in M. Boucher (1995).

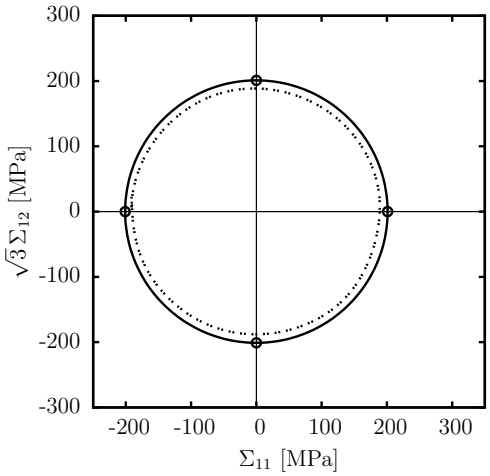

(a) Initial yield surface

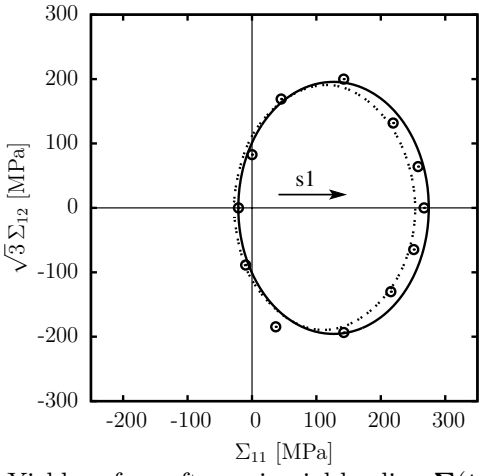

(b) Yield surface after uni-axial loading $\boldsymbol{\Sigma}(t_1) = \Sigma_{11}(t_1)\,\mathbf{e}_1 \otimes \mathbf{e}_1$

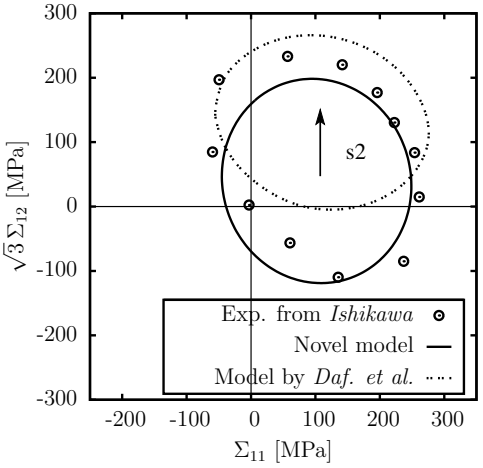

(c) Yield surface after tension unloading to 100 [MPa] and subsequent torsional loading $\boldsymbol{\Sigma}(t_2) = 100\ \text{MPa}\,\mathbf{e}_1 \otimes \mathbf{e}_1 + \Sigma_{12}(t_2)\,\text{sym}(\mathbf{e}_1 \otimes \mathbf{e}_2)$

Figure 4: Evolution of the yield surface for the stainless steel SUS304 subjected to simple tension, followed by torsion. Novel model: solid line. Model proposed in Dafalias et al. (2003); Schick (2004): dashed line. The symbols are associated with the experimental measurements reported in Ishikawa (1997).

yield surface's curvature in loading direction and in the opposite direction. In spite of the complexity of the final model, its derivation is indeed canonical. To be more precise, it falls into the range of so-called *generalized standard material*, i.e., the model is uniquely defined by means of a Helmholtz energy, a yield function and plastic potentials associated with the evolution equations. Concerning the latter, the design of the new potentials corresponding to distortional hardening was presented in detail. It turns out that quadratic potentials are sufficient. Although such potentials share some similarities to the classical Armstrong-Frederick-type law, they are indeed not equivalent. Based on a convexity analysis of the yield surface, the three model parameters related to distortional hardening could be naturally bounded. Three different examples demonstrated the predictive capabilities of the novel framework. In this connection, the range of application varied from high-strength aluminum alloys to stainless steel.

Acknowledgements

Financial support from the German Research Foundation (DFG) via SFB/TR TRR 30, project B4, is gratefully acknowledged. Furthermore, financial support for the first author was provided by the China Scholarship Council. This funding is also gratefully acknowledged.

AppendixA. Model parameters calibrated for the Al alloy and steel

Baltov, A., Sawczuk, A., 1965. A rule of anisotropic hardening. Acta Mechanica 1, 81–92.

Barthel, C., Levkovitch, V., Svendsen, B., 2008. Modeling of sheet metal forming processes taking into account distortional hardening. International Journal of Material Forming 1, 105–108.

Boers, S., Schreurs, P., Geers, M., Levkovitch, V., Wang, J., Svendsen, B., 2010. Experimental characterization and model indentification of directional hardening effects in metals for complex strain path changes. International Journal of Solids and Structures 47, 1361–1374.

Bruhns, O., Xiao, H., Meyers, A., 1999. Self-consistent eulerian rate type elastoplasticity models based upon the logarithmic stress rate. International Journal of Plasticity 15 (5), 479 – 520.

Material parameters of novel model for Al alloy 6061-T6511 - Subsection 3.4, Fig. 2, Lamé constants: $\lambda = 51.8$ GPa, $\mu = 25.9$ GPa

Q_0 [MPa]	c_{iso}	Q_{iso}^{∞} [MPa]	b_{kin}	c_{kin} [MPa]
93.9	0.0	0.0	91.9	18800

b_{D}	b_{L}	b_{C} $[\text{MPa}]^{-1}$	c_{D} $[\text{MPa}]^{-1}$	c_{L} $[\text{MPa}]^{-1}$
-44.5	-5.6	0.144	40	5

Material parameters of novel model for Al alloy 2024 - Subsection 3.4, Fig. 3, Lamé constants: $\lambda = 55.0$ GPa, $\mu = 27.5$ GPa

Q_0 [MPa]	c_{iso}	Q_{iso}^{∞} [MPa]	b_{kin}	c_{kin} [MPa]
155	$4.79 \cdot 10^{-2}$	8.85	108	14500

b_{D}	b_{L}	b_{C} $[\text{MPa}]^{-1}$	c_{D} $[\text{MPa}]^{-1}$	c_{L} $[\text{MPa}]^{-1}$
$1.31 \cdot 10^{-1}$	$3.72 \cdot 10^{-1}$	$5.31 \cdot 10^{-3}$	10.9	1.25

Material parameters of novel model for stainless steel SUS304 - Subsection 3.3, Fig. 4, Lamé constants: $\lambda = 98.0$ GPa, $\mu = 73.9$ GPa

Q_0 [MPa]	c_{iso}	Q_{iso}^{∞} [MPa]	b_{kin}	c_{kin} [MPa]
164	$1.11 \cdot 10^{-1}$	3.96	26.6	3240

b_{D}	b_{L}	b_{C} $[\text{MPa}]^{-1}$	c_{D} $[\text{MPa}]^{-1}$	c_{L} $[\text{MPa}]^{-1}$
$-8.50 \cdot 10^{-1}$	$-5.29 \cdot 10^{-1}$	0.0	112	$2.90 \cdot 10^{-1}$

Table A.2: Model parameters for Al alloys and for steel

Coleman, B., Gurtin, M., 1967. Thermodynamics with internal state variables. Journal of Chemical Physics 47, 597–613.

Dafalias, Y. F., 1979. Anisotropic hardening of initially orthotropic materials. Journal of Applied Mathematics and Mechanics 59, 437–446.

Dafalias, Y. F., Schick, D., Tsakmakis, C., 2003. A simple model for describing yield surface evolution during plastic flow. In: Deformation and Failure in Metallic Materials (Lecture Notes in Applied and Computational Mechanics). Springer, Berlin.

Feigenbaum, H., Dafalias, Y., 2007. Directional distortional hardening in metal plasticity within thermodynamics. International Journal of Solids and Structures 44, 7526–7542.

Feigenbaum, H., Dafalias, Y., 2008. Simple Model for Directional Distortional Hardening in Metal Plasticity within Thermodynamics. Journal of Engineering Mechanics 134 (9), 730–738.

Haddadi, H., Bouvier, S., Banu, M., Maier, C., Teodosiu, C., 2006. Towards an accurate description of the anisotropic behaviour of sheet metals under large plastic deformations: Modelling, numerical analysis and indentification. International Journal of Plasticity 22, 2226–2271.

Hiwatashi, S., Bael, A., Houtte, P., Teodosiu, C., 1998. Prediction of forming limit strains under strain-path changes: application of an anisotropic model based on texture and dislocation structure. International Journal of Plasticity 14 (7), 647–669.

Homayonifar, M., Mosler, J., 2012. Efficient modeling of microstructure evolution in magnesium by energy minimization. International Journal of Plasticity 28, 1–20.

Ishikawa, H., 1997. Subsequent yield surface probed from its current center. International Journal of Plasticity 13, 533–549.

Khan, A. S., Kazmi, R., Pandey, A., Stoughton, T., 2009. Evolution of subsequent yield surfaces and elastic constants with finite plastic deformation. part-i: A very low work hardening aluminum alloy (al6061-t6511). International Journal of Plasticity 25 (9), 1611 – 1625.

Lee, E., 1969. Elastic-plastic deformation at finite strains. Journal of Applied Mechanics 36, 1–6.

Lemaitre, J., 1985. A continuous damage mechanics model for ductile fracture. J. Eng. Mat. Techn. 107, 83–89.

M. Boucher, P. Cayla, J. P. C., 1995. Experimental studies of yield surfaces of aluminium alloy and low carbon steel under complex biaxial loadings. Eur. J. Mech., A/Solids 14, 1–17.

Mandel, J., 1971. Plasticite classique et viscoplasticitite. CISM.

Mekonen, M. N., Steglich, D., Bohlen, J., Letzig, D., Mosler, J., 2012. Mechanical characterization and constitutive modeling of mg alloy sheets. Materials Science and Engineering: A 540 (0), 174 – 186.

Miehe, C., Schotte, J., Lambrecht, M., 2002. Homogenization of inelastic solid materials at finite strains based on incremental minimization principles. application to the texture analysis of polycrystals. Journal of the Mechanics and Physics of Solids 50 (10), 2123 – 2167.

Nebebe, M., Bohlen, J., Steglich, D., Letzig, D., 2009. Mechanical characterisation of Mg alloys and model parameter identification for sheet forming simulations. International Journal of Material Forming 2, 53–56, 10.1007/s12289-009-0437-5.

Noman, M., Clausmeyer, T., Barthel, C., Svendsen, B., Huetink, J., Riel, M., 2010. Experimental characterization and modeling of the hardening behavior of the sheet steel LH800. Materials Science and Engineering A 527, 2515–2526.

Ortiz, M., Popov, E., 1983. Distortional Hardening Rules for Metal Plasticity. Journal of Engineering Mechanics 109 (4), 1042–1057.

Peeters, B., Kalidindi, S., Teodosiu, C., Houtte, P., Aernoudt, E., 2002. A theoretical investigation of the influence of dislocation sheets on evolution of yield surfaces in single-phase B.C.C. polycrystals. Journal of the Mechanics and Physics of Solids 50, 783–807.

Pietryga, M. P., Vladimirov, I. N., Reese, S., 2012. A finite deformation model for evolving flow anisotropy with distortional hardening including experimental validation. Mechanics of Materials 44, 163 – 173.

Plesek, J., Feigenbaum, H., Dafalias, Y., 2010. Convexity of Yield Surface with Directional Distortional Hardening Rules. Journal of Engineering Mechanics 136 (4).

Schick, D., 2004. Anisotropic plasticity and viscoplasticity. Ph.D. thesis, TU Darmstadt.

Shi, B., Mosler, J., 2013. On the macroscopic description of yield surface evolution by means of distortional hardening models: Application to magnesium. International Journal of Plasticity 44, 1–22.

Simo, J., Hughes, T., 1998. Computational Inelasticity. Vol. 7 of Interdisciplinary Applied Mathematics. Springer-Verlag New York, Inc.

Simo, J. C., 1998. Numerical analysis of classical plasticity. Vol. IV of Handbook for numerical analysis. Elsevier, Amsterdam.

Wang, J., Levkovitch, V., Reusch, F., Svendsen, B., Huetink, J., Riel, M., 2008. On the modeling of hardening in metals during non-proportional loading. International Journal of Plasticity 24, 1039–1070.

Xiao, H., Bruhns, O., Meyers, A., 2000. A consistent finite elastoplasticity theory combining additive and multiplicative decomposition of the stretching and the deformation gradient. International Journal of Plasticity 16 (2), 143 – 177.